Petroleum Science 19 (2022) 296–308

Contents lists available at ScienceDirect

Petroleum Science

journal homepage: www.keaipublishing.com/en/journals/petroleum-science

Original Paper

Numerical investigation on the effect of depletion-induced stress reorientation on infill well hydraulic fracture propagation

Feng-Shou Zhang [a, b], Liu-Ke Huang [a, b, c, *], Lin Yang [a, b], Egor Dontsov [d], Ding-Wei Weng [e], Hong-Bo Liang [e], Zi-Rui Yin [a, b], Ji-Zhou Tang [f, g]

[a] Key Laboratory of Geotechnical & Underground Engineering of Ministry of Education, Tongji University, Shanghai, 200092, China
[b] Department of Geotechnical Engineering, College of Civil Engineering, Tongji University, Shanghai, 200092, China
[c] State Key Laboratory of Geomechanics and Geotechnical Engineering, Institute of Rock and Soil Mechanics, Chinese Academy of Sciences, Wuhan, 430071, China
[d] ResFrac Corporation, Palo Alto, CA, 94301, USA
[e] PetroChina Research Institute of Petroleum Exploration and Development, Langfang, 065007, China
[f] State Key Laboratory of Marine Geology, Tongji University, Shanghai, 200092, China
[g] School of Ocean and Earth Science, Tongji University, Shanghai, 200092, China

ARTICLE INFO

Article history:
Received 10 February 2021
Accepted 13 August 2021
Available online 10 September 2021

Edited by Xiu-Qiu Peng

Keywords:
Infill well
Depletion
Hydraulic fracture
Stress reorientation
Asymmetry fracture

ABSTRACT

Depletion-induced stress change causes the redistribution of stress field in reservoirs, which can lead to the reorientation of principal stresses. Stress reorientation has a direct impact on fracture propagation of infill wells. To understand the effect of stress reorientation on the propagation of infill well's fractures, an integrated simulation workflow that combines the reservoir flow calculation and the infill well hydraulic fracturing modeling is adopted. The reservoir simulation is computed to examine the relationship between the extent of stress reversal region and reservoir properties. Then, the hydraulic fracturing model considering the altered stress field for production is built to characterize the stress evolution of secondary fracturing. Numerical simulations show that stress reorientation may occur due to the decreasing of the horizontal stresses in an elliptical region around the parent well. Also, the initial stress difference is the driving factor for stress reorientation. However, the bottom hole pressure, permeability and other properties connected with fluid flow control timing of the stress reorientation. The decrease of the horizontal stresses around the parent well lead to asymmetrical propagation of a hydraulic fracture of the infill well. The study provides insights on understanding the influence of stress reorientation to the infill well fracturing treatment and interference between parent and infill wells.

1. Introduction

Infill well fracturing technology is able to improve the reservoir's production efficiency. Figuring out the stress change caused by parent well's fracturing process and subsequent production is important for implementing infill well fracturing. The opening of the fracture and decrease of the pore pressure alter the stress field around the wellbore and fractures. Consequently, the direction of the maximum and minimum horizontal stressed is deviated from the original trend and the fracture propagation is influenced. Thus, it is vital to explore the mechanism behind the fracture propagation under the effect of stress reorientation. This topic is first studied by Mack and Elbel (1994) who find that along with the production, stresses within the depletion region decrease and the stress components in the direction parallel to the fracture decrease faster than the stress components in the direction perpendicular to the fracture. A reorientation theory is summarized based on this finding. This theory is improved by Siebrits et al. (1998) who bring up the concept of stress reversal region and analyze the influence of various reservoir properties by using a 3D simulation model.

The concept of stress reversal region is illustrated in Fig. 1. At the beginning, the direction of the maximum horizontal stress (σ_{hmax}) is parallel to the initial vertical fracture plane. During production, the stress parallel to the hydraulic fracture plane decreases faster

* Corresponding author. Key Laboratory of Geotechnical & Underground Engineering of Ministry of Education, Tongji University, Shanghai, 200092, China.
E-mail address: liukehuang@tongji.edu.cn (L.-K. Huang).

https://doi.org/10.1016/j.petsci.2021.09.014

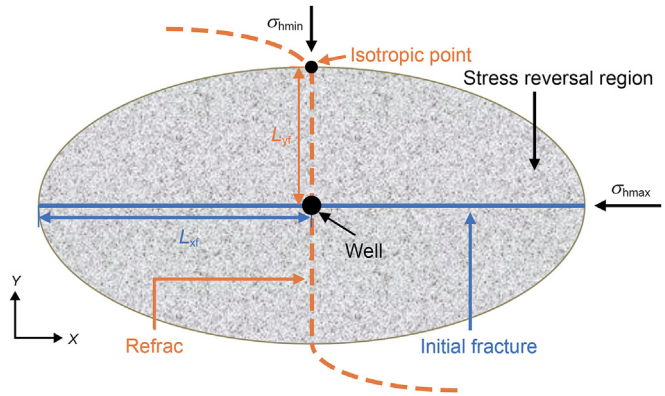

Fig. 1. Concept of stress reversal region (modified from Siebrits et al., 1998).

than the stress in the direction perpendicular to it. Therefore, this alteration makes it possible to overcome the initial horizontal stress contrast between the minimum horizontal stress (σ_{hmin}) and σ_{hmax}. As a result, the stress reversal region develops around the fractures. In this case, refracturing at the same place could create a new fracture which initially propagates orthogonally to the initial fracture. Once it extends beyond the "isotropic point" at which the stresses in the two perpendicular directions are equal, the maximum principal stress switches back to its original direction, causing the secondary fracture to rotate back to be parallel to the initial fracture. The refracturing treatment makes use of this phenomenon so that the new fractures might intersect the region with more residual oil and higher fluid pressure (Elbel and Mack, 1993; Zhang and Dontsov, 2018). However, this phenomenon does not always occur in the field. The stress reorientation depends on many factors including the initial horizontal stress contrast, permeability, production rate and pore pressure drawdown (Li et al., 2006; Tan et al., 2020; Zeng et al., 2015; Zhai and Sharma, 2007; Zhu et al., 2021). In order to better understand the hydraulic fractures' deviation within the altered stress field, Berchenko and Detournay (1997) defined two dimensionless quantities: stress deviator and dimensionless time to minimize the number of independent parameters. Many simulation models are built to analyze the relationship among these factors and the extent of the stress reversal region, but few considered the coupled poroelastic mechanical effect on the stress reorientation (Aghighi et al., 2009; Chen and Teufel, 2001; Lin et al., 2020; Roussel, 2011). The opening of a propped fracture has been proved to be a source of the stress reorientation as well (Warpinski and Branagan, 1989). Roussel and Sharma (2010) discussed the effect of poroelastic stress and stress induced by mechanical opening of hydraulic fractures together instead of independently and found that they are dependent on each other in a complex way, rather than being simply additive.

One of the applications of the stress reorientation analysis is for infill well optimization. The key to a successful infill well fracturing is to make as large fracture surface area as possible and to penetrate less into the depleted zones. There are numerous previous works that focus on the fracture propagation within the perturbed stress field (Bruno and Nakagawa, 1991; Gao et al., 2019; Li et al., 2017; Zhang et al., 2015). All these studies demonstrate that non-uniform pore pressure field does affect the initiation and propagation process of hydraulic fractures. Recently, Gupta et al. (2012) uncovered that reservoir depletion from parent wells can have detrimental impacts on fracture propagation of infill wells, and subsequently lowers the well productivity. In particular, in the case of low horizontal stress anisotropy, the intermediate stress direction is shown to reorient parallel to the infill well, potentially leading to longitudinal fractures. Not only production from offset wells impacts fracture propagation in the infill region, but stimulation of the infill well has also been shown to affect production in the offset wells, either positively or negatively (Ajani and Kelkar, 2012; Gupta et al., 2012). In some cases, production in the offset wells may even be completely suppressed. Safari et al. (2017) proposed to take advantage of the *in-situ* stress changes to prevent interference between the wells. Within the stress reversal region, direction of the maximum principal stress is deviated, which means that the infill well fractures may be deviated away from the preexisting wells.

There is an extensive documentation of the pressure interference in shales aiming to achieve economic benefit of increased production from the infill well (Ajani and Kelkar, 2012; Sahai et al., 2012). But in the case of infill drilling, hydraulic connection might not be the limiting factor. Whether poroelastic stress interference plays a bigger role than fluid flow interference depends largely on the value of the *in-situ* stress contrast. In cases featuring large in situ horizontal anisotropy, stress reversal is unlikely to occur and fluid flow interference is then likely to dominate. Studying of the impact of pressure-induced stress changes on fracture propagation direction is by no means of recent interest (Berchenko and Detournay, 1997). In tight gas plays, poroelastic stress interference has been previously investigated and applied to the refracturing of vertical wells (Roussel, 2011; Roussel and Sharma, 2010; Siebrits et al., 1998; Tan et al., 2021; Tang et al., 2019; Warpinski and Branagan, 1989; Yi et al., 2020).

Nevertheless, prediction of the behavior of hydraulic fractures within the perturbed stress field is a challenging task. The main objective of this study is therefore to investigate the propagation process of the fractures within the nonuniform stress field. However, it is common not to simulate the hydraulic fracturing process and production with the same model because these two processes have different nature and occur at different time scales. Therefore, the following workflow that combines the advantages of finite difference method and distinct element method is applied in this study. It is possible to obtain the stress field which has already been altered by the depletion in reservoir model by using finite difference method and model the hydraulic fracturing process by using the distinct element method with the input of the altered stress field. Thus, this study contains two parts and the first step is to examine the relationship between the extent of stress reversal region and reservoir properties. A set of dimensionless parameters is introduced to quantify the impact of mechanical properties, production parameters and geometry of the fractures to the stress reorientation. The sensitivity analysis of these variables is performed to illustrate the best practice of the infill well fracturing treatment. Then, the fracture propagation from a horizontal infill well and its sensitivity to stress reorientation is investigated. This work provides some insights on understanding the influence of stress reorientation to the infill well fracturing treatment and interference between parent and infill wells.

2. Model setup

2.1. Numerical scheme

The finite difference method code FLAC3D is used to calculate the temporal and spatial evolution of the stress field in the vicinity of injection/production wells, which is able to simulate the rock deformation induced by pore pressure change(Itasca Consulting Group Inc, 2011). Two main mechanical processes are included in this simulation: (1) the effective stress varies with the pore pressure, which affect the response of the rock, and (2) the fluid pressure reacts to volumetric deformations of the rock. The following

equations considering Darcy's law, the fluid mass balance, mechanical constitutive laws and pore pressure are given to describe the hydro-mechanical coupling.

The fluid transport in a porous material is described by Darcy's law:

$$q_i = -k_{ij}^{a}\frac{\partial}{\partial x_k}\left(P-\rho_f x_k g_k\right) \tag{1}$$

where q_i is the specific discharge vector, P is pore pressure, ρ_f is fluid density, g_k is gravity vector. i (j, k) take the values 1, 2, 3. k_{ij}^{a} is apparent mobility coefficient, which is a function of fluid saturation.

The fluid mass balance is formulated as:

$$\frac{\partial \zeta}{\partial t} = -\frac{\partial q_i}{\partial x_i} + q_v \tag{2}$$

where q_v is the volumetric fluid source intensity. ζ is the variation of fluid content or variation of fluid volume per unit volume of porous material.

The balance of momentum has the form:

$$\frac{1}{\rho}\frac{\partial \sigma_{ij}}{\partial x_j} + g_i = -\frac{\mathrm{d}\dot{u}_i}{\mathrm{d}t} \tag{3}$$

where σ_{ij} is stress, $\dot{u}_i$ is velocity, t is time. $\rho = \varphi\rho_f + \rho_d$ is the bulk density, φ is porosity, and ρ_d is the density of the dry porous material.

The variation of fluid volume is determined by P and ε (mechanical volumetric strains). The response equation for the pore fluid is expressed as:

$$\frac{1}{M}\frac{\partial P}{\partial t} = \frac{\partial \zeta}{\partial t} - \alpha\frac{\partial \varepsilon}{\partial t} \tag{4}$$

where M is Biot modulus, and α is Biot coefficient.

The elastic relations (constitutive law) that relate effective stresses to strains are formulated as (small strain):

$$\sigma_{ij} - \sigma_{ij}^{0} + \alpha\left(P-P^{0}\right)\delta_{ij} = 2G\dot{\varepsilon}_{ij}\Delta t + \left(K-\frac{2}{3}G\right)\dot{\varepsilon}_{kk}\delta_{ij}\Delta t \tag{5}$$

Where $\dot{\varepsilon}_{ij}$ is the strain rate, δ_{ij} is the Kronecker delta, Δt is time step. K and G are bulk modulus and shear modulus of the porous material, respectively. The superscript ^{0} refers to the initial state.

The relation between strain rate and velocity gradient (compatibility equation) is:

$$\dot{\varepsilon}_{ij} = \frac{1}{2}\left(\frac{\partial \dot{u}_i}{\partial x_j} + \frac{\partial \dot{u}_j}{\partial x_i}\right) \tag{6}$$

The three-dimensional distinct element code 3DEC is employed in this study for the hydraulic fracturing modeling of an infill well, which is suitable for modeling a discontinuous medium that consists of blocks and discontinuities (Cundall, 1988; Hart et al., 1988; Itasca Consulting Group Inc, 2016). In this study, the rock mass is modeled as an assemblage of deformable rock blocks. Each individual block is discretized into an internal mesh consisting of tetrahedral zones that is used for finite difference calculations, while the joints represent interactions between the rock blocks through their boundaries. An explicit time stepping algorithm is employed for the mechanical calculation. At each time step, the constitutive equations are solved to calculate the stress in the whole domain. With the updated nodal force based on the updated stresses, the equations of motion are solved at all grid points to calculate velocities that are utilized to obtain the new strain rates. The integration of the equations of motion provides the new block positions and contact displacement increments. The joint forces are then updated based on the joint constitutive laws and applied to the blocks in the next time step. The fluid flow through the joints is modeled by the two-way hydro-mechanical coupled analysis in which the joint aperture and hydraulic conductivity depend on the mechanical deformation of the rock blocks, while the fluid pressure also affects the mechanical deformation of the rock blocks. The propagation of fluid-driven fractures is implemented by breaking the joints along the predefined joint plane in either tensile or shear mode (Huang et al. 2019, 2020; Yin et al., 2020; Zhang et al., 2019; Zhang and Mack, 2017).

2.2. Model geometry

A reservoir production model is built to get the altered stress field by using FLAC3D. The model is implemented in three dimensions and contains a rectangular hydraulic fracture. The model configuration is illustrated in Fig. 2 and the reservoir properties that are used for the base case are summarized in Table 1.

The model consists of three layers including two bounding layers and one reservoir layer as the pay zone. The two bounding layers have the same heights and the layer of the reservoir has a variable height since the thickness of the pay zone may influence the extent of the stress reversal region (Siebrits et al., 1998). The reservoir properties are taken from the field case of Ordos Basin, China. The mechanical properties (E_b, ν_b) of the layers bounding the reservoir are different from the properties of the pay zone layer (E_p, ν_p). The flow is restricted to the reservoir layer by applying an extremely low permeability in the two bounding layers. The whole model is assumed to be elastic, homogeneous and isotropic except that the permeability is different in the horizontal and vertical directions. The boundary conditions for the model are illustrated in Fig. 3 and can be summarized as:

- Fixed pore pressure at the face of the fractures
- Constant stress applied along the outer boundary of the domain: $\sigma_{zz} = \sigma_v$, $\sigma_{xx} = \sigma_{hmax}$, $\sigma_{yy} = \sigma_{hmin}$
- The outer boundary of the model is impermeable
- Fixed bottom hole pressure for production

Considering the effect of boundary, the predefined hydraulic fractures are placed at a distance from the boundary equal to at least three times of the half fracture length in order to avoid the impact of boundary condition on the extent of the stress reversal region. Constant *in-situ* stresses are applied at the outer boundary of the model. The bottom of the model is fixed. The hydraulic fracture is created by firstly splitting the grid points along the specified fracture surface and then by applying pressure to the two fracture surfaces. Consequently, a rectangular fracture volume is formed. Then, beam elements are used as proppant to make sure that the fractures remain open during depletion.

The *in-situ* stresses in the hydraulic fracturing model are defined by importing the stress field calculated by reservoir model. The reservoir and surrounding rock matrix in the hydraulic fracturing model are assumed to be elastic, homogeneous, and isotropic. Fig. 4 shows the 3D model constructed for the fracture propagation analysis. The properties used in the hydraulic fracturing model are the same as the ones used in the reservoir model. The hydraulic fracturing model has smaller dimensions compared with the model in the reservoir model in order to assure that the altered stress field from the reservoir model can cover the whole region. The hydraulic fracturing model contains one infill and one parent well. The two

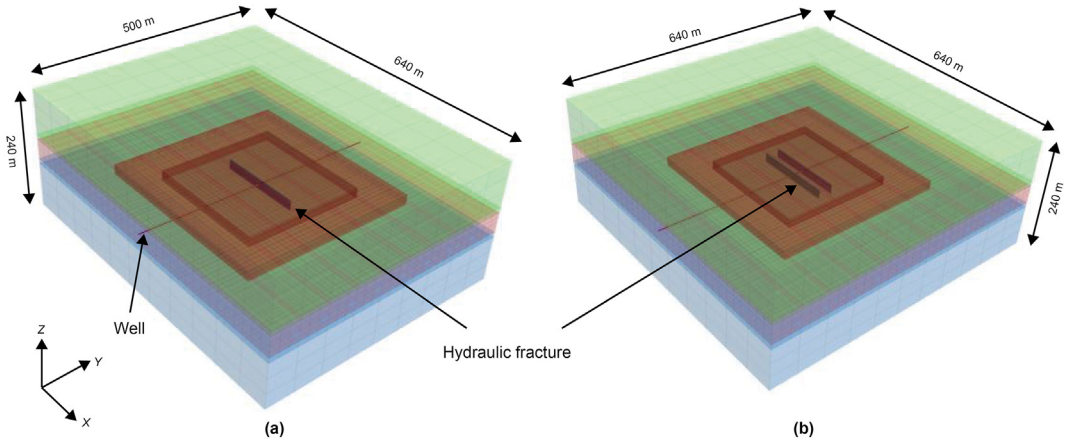

Fig. 2. The configuration of reservoir production model, **a** with a single hydraulic fracture, **b** with two hydraulic fractures.

Table 1
Geomechanical and reservoir properties for computation of the stress evolution due to depletion.

Parameters	Value	Parameters	Value
Depth, m	−1600~-1840	Young's modulus, GPa	20.1
Horizontal permeability, m^2	1.90×10^{-16}	Poisson's ratio	0.16
Vertical permeability, m^2	1.90×10^{-21}	Biot coefficient	0.783
Bottom hole pressure, MPa	10	Porosity	0.108
Minimum horizontal stress, MPa	27.52	Pore pressure, MPa	15.14
Maximum horizontal stress, MPa	28.66	Viscosity, Pa•s	0.00104
Vertical stress gradient, MPa/m	0.024		

wells are parallel to each other and have a distance of 170 m between them. The fracturing fluid is assumed to be incompressible.

2.3. Dimensionless parameters

The former research has proven that there are typically 4 types of dimensionless parameters affecting reservoir's stress reorientation: dimensionless time, dimensionless stress deviator, dimensionless fracture height ratio and dimensionless shear modulus ratio (Berchenko and Detournay, 1997; Roussel, 2011; Siebrits et al., 1998).

It has been well known that the stress reorientation phenomenon is influenced by many parameters, such as the reservoir geomechanical properties, wellbore pressure, horizontal stress contrast, and the bounding layer properties. In order to minimize the number of relevant variables, Berchenko and Detournay (1997) defined two dimensionless parameters: τ, the dimensionless time; Π, the ratio of the initial deviation stress to the difference between initial reservoir pressure and well pressure.

Dimensionless time:

$$\tau = \frac{4ct}{L_{xf}^2} = \frac{4k}{S}\frac{t}{L_{xf}^2} = \frac{4kt}{\mu L_{xf}^2\left(c_f\varphi + \frac{\alpha(1+\nu)(1-2\nu)}{(1-\nu)E}\right)} \tag{7}$$

where τ is the dimensionless time, c is the fluid diffusivity, t is time, L_{xf} is the half length of the hydraulic fracture, k is permeability, μ is fluid viscosity, φ is porosity, S is hydraulic storage, ν is Possison's ratio, and E is the Young's modulus.

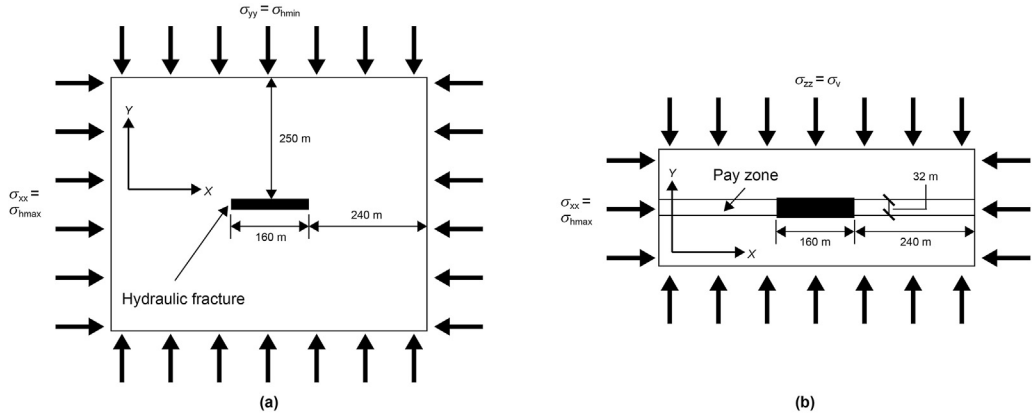

Fig. 3. a Boundary conditions for the reservoir model (XY-plane) and **b** geometry of a vertical fracture in the reservoir model (XZ-plane).

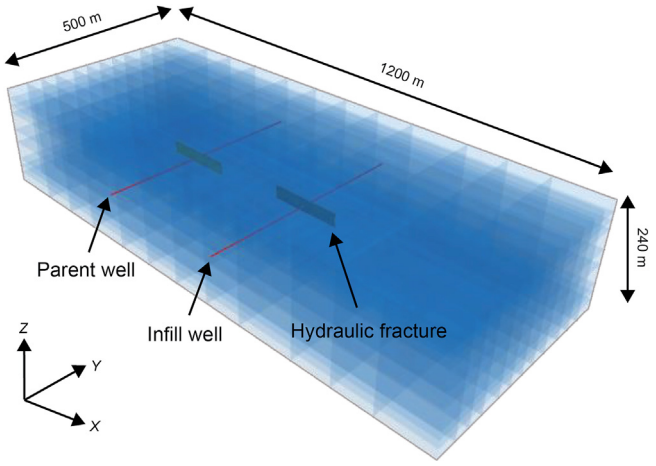

Fig. 4. The configuration of the hydraulic fracturing model.

Dimensionless stress deviator:

$$\prod = \frac{S_0}{\sigma_*} = \frac{S_0}{\eta P_*} = \frac{\sigma_{\mathrm{hmax}} - \sigma_{\mathrm{hmin}}}{\frac{\alpha(1-2\nu)}{1-\nu}|P_0 - P_{\mathrm{w}}|} \tag{8}$$

where Π is the dimensionless stress deviator, P_0 is the initial reservoir pore pressure, and P_{w} is the bottom hole pressure. S_0 is far-field stress deviator. σ_* is characteristic stress. When bottom hole pressure is kept constant, P_* equals difference between far-field pressure and bottom hole pressure.

For 2D geometry, it is concluded that the production induced stress is scaled by the dimensionless stress deviator and depends only on the dimensionless time. But for the case of 3D geometry, two new dimensionless parameters are introduced. The numerical results by Siebrits et al. (1998) show that the layer bounding the reservoir affects stress reorientation. Thus, Roussel (2011) proposed two additional parameters to take into account the influence of the reservoir height and the mechanical characteristics of the bounding layers.

Dimensionless fracture height ratio:

$$\gamma = \frac{h_{\mathrm{f}}}{L_{\mathrm{f}}} \tag{9}$$

where γ is the dimensionless fracture height ratio, h_{f} is the height of hydraulic fracture, L_{f} is the length of hydraulic fracture.

Dimensionless shear modulus ratio:

$$\beta = \frac{G_{\mathrm{b}}}{G_{\mathrm{p}}} \tag{10}$$

where β is the dimensionless shear modulus ratio, G_{b} is the shear modulus of bounding layer, G_{p} is the shear modulus of pay zone.

Initial maximum and minimum stresses both decrease during production due to depletion of the reservoir. Since the maximum stress decreases faster, at some distance from the fracture along the y-axis the maximum and minimum stresses become equal. This corresponds to the isotropic point, whereby the extent of stress reversal region is defined by the distance L_{yf} from the fracture to the isotropic point. Position of the isotropic point varies with the dimensionless time. And it is also clear that this distance is related to the fracture length. Therefore, it is better to use a dimensionless quantity to define the extent of the stress reversal region:

$$\lambda = \frac{L_{\mathrm{yf}}}{h_{\mathrm{f}}} \tag{11}$$

and it is defined as a function of stress deviator Π, dimensionless fracture height ratio γ and dimensionless shear modulus ratio β.

3. Numerical results of stress reorientation

Fig. 5 illustrates a typical stress reorientation pattern and provides a better perspective to the extent of the stress reversal region. Fig. 5 shows a top view ($z = 0$) of the simulation model, in which the well has been producing for $\tau = 100$ with the parameters specified in Table 1. The white dashed contour line agrees with the demonstration model of Siebrits et al. (1998) (Fig. 1), but outside of the elliptical reversal region, there are still two wings, which represent a difference from the former research. The occurrence of stress reorientation comes from two aspects: mechanical stress reorientation and poroelastic stress reorientation, which will be discussed respectively in the following sections.

3.1. Mechanical stress orientation

Creation of a hydraulic fracture generates an additional stress that is mostly perpendicular to the fracture face. Fig. 6 shows direction of the maximum horizontal principal stress after fracture opening and clearly demonstrates that open fractures can significantly alter the stress contrast and cause the direction of maximum horizontal principal stress to rotate 90° in the vicinity of the fracture. This phenomenon is called mechanical reorientation. For mechanical reorientation, the appearance of stress reversal region is caused by opening of the hydraulic fracture. The net pressure is directly applied on the face of the fracture and, as stated before, the hydraulic fracture is assumed as two planes. Therefore, the stress around the fracture increases and the stress parallel to the net pressure increase much more compared to the stress perpendicular to the direction of net pressure. As a result, the stress reversal region appears and because the change of stress is caused by the force

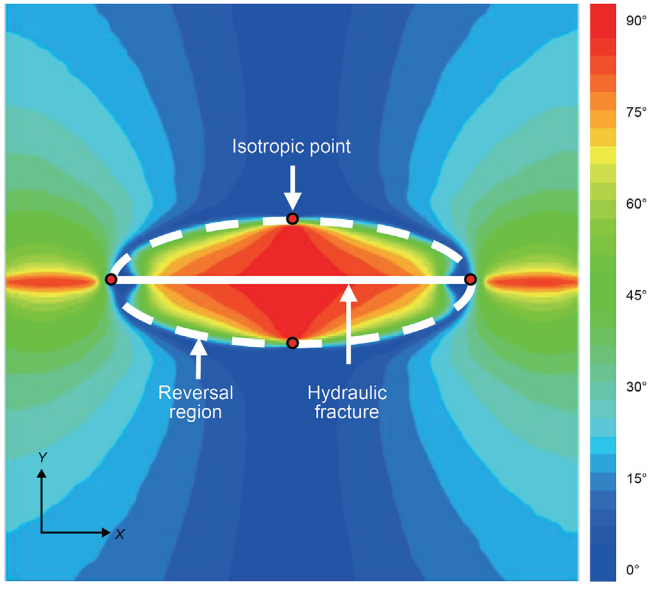

Fig. 5. Contour of the maximum horizontal stress direction after $\tau = 100$ of production (90° represents the direction that is perpendicular to the fracture and 0° represents the direction that is parallel to the fracture. The white lines indicate the direction of maximum horizontal stress).

applied on the fracture planar face, the stress reversal region is nearly rectangular. However, poroelastic reorientation is induced by the decrease of pore pressure and, after years' production, pore pressure field distributes in elliptical form. Thus, the stress reversal region is nearly elliptical, as shown in Fig. 5.

The rotation angle of the maximum horizontal principal stress is 90° in this reversal zone, except the tip of the fracture. This is because the magnitude of the shear stress is small, as indicated in Fig. 7. Consequently, directions of the horizontal principal stresses are along the *x*-axis and *y*-axis. Thus, it is found that within this reversal zone the maximum horizontal stress is along the *y*-axis and the minimum horizontal principal is along the *x*-axis. On the other hand, the stresses in the direction parallel to the fracture (σ_{xx}) and perpendicular to the fracture (σ_{yy}) can represent the impact of mechanical reorientation. So, it is convenient to use the differences of σ_{yy} and σ_{xx} along the *y*-axis to quantify the degree of stress reversal. The generated stress contrast decreases as the distance from the fracture increases and the point at which the generated stress contrast equals to zero is the isotropic point.

Extent of stress reorientation depends on the mechanical properties of reservoir and is more significant if the difference between the initial maximum and minimum horizontal principal stresses is small. At the beginning of depletion, Fig. 8a shows that the additional force (P_{net}) that is applied on the rock in the direction normal to the fracture face increases σ_{yy} and its influence on σ_{xx} is much smaller. Compressive stresses and strains have a negative sign in the model. So, if the increase of σ_{yy} is sufficiently large, the generated stress contrast will overcome the initial horizontal stress contrast to create a zone with abs(σ_{yy})>abs(σ_{xx}). Therefore, the smaller the horizontal stress contrast is, the easier this alteration will be accomplished. In addition to the initial horizontal stress contrast, the reservoir's mechanical properties also affect stress reorientation. As shown in Fig. 8b, a bigger stress contrast is generated in a reservoir with a lower Poisson's ratio. A low Poisson's ratio implies that the deformation in the direction parallel to the fracture is small compared to the deformation perpendicular to the fracture. Besides, Poisson's ratio also influences the production process which will be discussed in the next section.

The extent of the stress reversal region is directly proportional to the fracture's dimensions. Several height values are tested in order to determine the relationship between the two variables. Fig. 9 show that as the value of h_f/h_r (h_r equals the reservoir height)

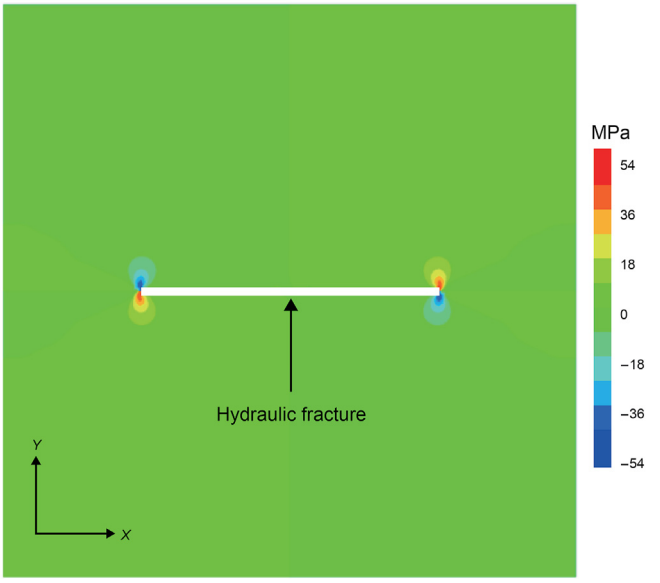

Fig. 7. Contour of the shear stress around a single propped-open fracture.

increases, the generated stress contrast increases too. However, the fracture heights are different in Fig. 9a, but the height ratios are all equal to 1.0. Even if the height of the fracture increases for the constant height ratio, the generated stress contrast keeps the same value.

3.2. Poroelastic stress reorientation

Production from the reservoir generates nonuniform pore pressure in the formation and also alters the stress field due to the poroelastic effect. This phenomenon is called poroelastic stress reorientation. Our investigation aims to answer why stress reorientation happens and how this altering stress field evolves through time.

First, the depletion induced pore pressure gradient is mainly responsible for this phenomenon (Fig. 10). This nonuniform pore pressure field makes the stress field all decrease and the horizontal stresses in the direction perpendicular to the fracture and in the

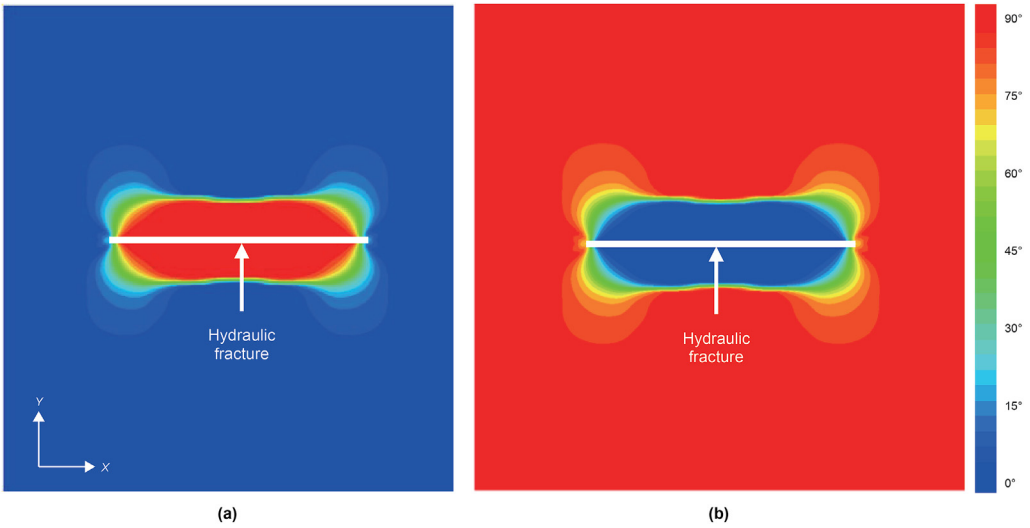

Fig. 6. a Direction of the maximum horizontal principal stress around a single propped-open fracture. **b** Direction of the minimum horizontal principal stress around a single propped-open fracture.

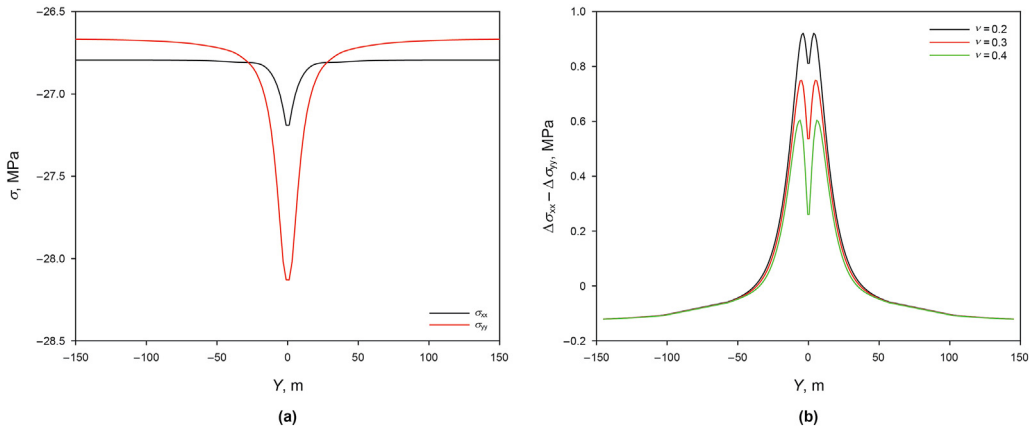

Fig. 8. **a** The stress change induced by the opening of a hydraulic fracture, **b** effect of Poisson's ratio to the mechanical stress reorientation.

direction parallel to the fracture decrease in different speed. Based on Hooker's law and Biot's poroelasticity theory (Biot, 1955), it's convenient to get the relationship between increment of stress and pore pressure,

$$\begin{bmatrix} \sigma'_{xx} \\ \sigma'_{yy} \\ \sigma'_{zz} \end{bmatrix} = \frac{E}{(1+\nu)(1-2\nu)} \begin{bmatrix} 1-\nu & \nu & \nu \\ \nu & 1-\nu & \nu \\ \nu & \nu & 1-\nu \end{bmatrix} \begin{bmatrix} \varepsilon_x \\ \varepsilon_y \\ \varepsilon_z \end{bmatrix} \tag{12}$$

Assuming that the vertical stress $\sigma_{zz} = -\sigma_v$ does not change, it is easy to get the following relationship,

$$\begin{bmatrix} \Delta\sigma_{xx} \\ \Delta\sigma_{yy} \\ 0 \end{bmatrix} - \alpha\Delta P \begin{bmatrix} 1 \\ 1 \\ 1 \end{bmatrix} = \frac{E}{(1+\nu)(1-2\nu)} \begin{bmatrix} 1-\nu & \nu & \nu \\ \nu & 1-\nu & \nu \\ \nu & \nu & 1-\nu \end{bmatrix} \times \begin{bmatrix} \Delta\varepsilon_x \\ \Delta\varepsilon_y \\ \Delta\varepsilon_z \end{bmatrix} \tag{13}$$

After solving the above equations, we obtain,

$$\begin{cases} \Delta\sigma_{xx} = \alpha\Delta P + \dfrac{E}{(1+\nu)(1-2\nu)}\left[(1-\nu)\Delta\varepsilon_x + \nu\Delta\varepsilon_y + \nu\Delta\varepsilon_z\right] \\ \Delta\sigma_{yy} = \alpha\Delta P + \dfrac{E}{(1+\nu)(1-2\nu)}\left[\nu\Delta\varepsilon_x + (1-\nu)\Delta\varepsilon_y + \nu\Delta\varepsilon_z\right] \end{cases} \tag{14}$$

$$\Delta\sigma_{xx} - \Delta\sigma_{yy} = \frac{E}{(1+\nu)}\left(\Delta\varepsilon_x - \Delta\varepsilon_y\right) \tag{15}$$

According to Eq. (14), the induced stress consists of two parts. One part is the change of pore pressure and the other part is deformation caused by the change of effective stress. The two components have opposite effect on the rock mass. The decrease of pore pressure is like unload to decrease the stress around the fracture. However, the deformation induced by fluid flow makes the rock mass more compacted, which means the effective stress arises. Especially, the deformation in the direction parallel to the fracture is different than that in the direction perpendicular to the fracture. Fig. 11 shows the contour of the difference of strain incremental ($\Delta\varepsilon_{xx}-\Delta\varepsilon_{yy}$) around a single fracture at different time. There is an elliptical region that satisfies the condition ($\Delta\varepsilon_{xx}>\Delta\varepsilon_{yy}$). In other words, in this region the horizontal stresses in the direction parallel to the fracture decrease faster or increases slower than the horizontal stresses in the direction perpendicular to the fracture. Consequently, a stress reversal region occurs.

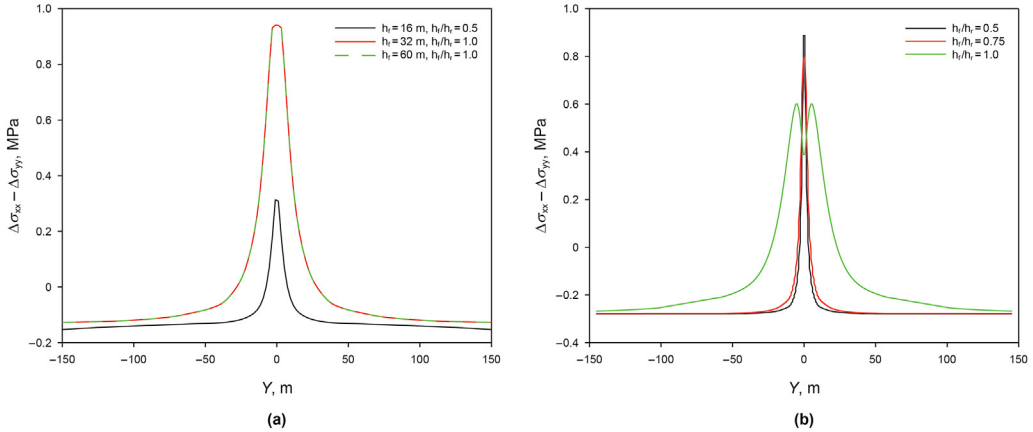

Fig. 9. **a** Generated stress contrast for different fracture heights and ratios of fracture height to reservoir height. **b** Generated stress contrast for different height ratios (h_f/h_r = 0.5, 0.75,1.0).

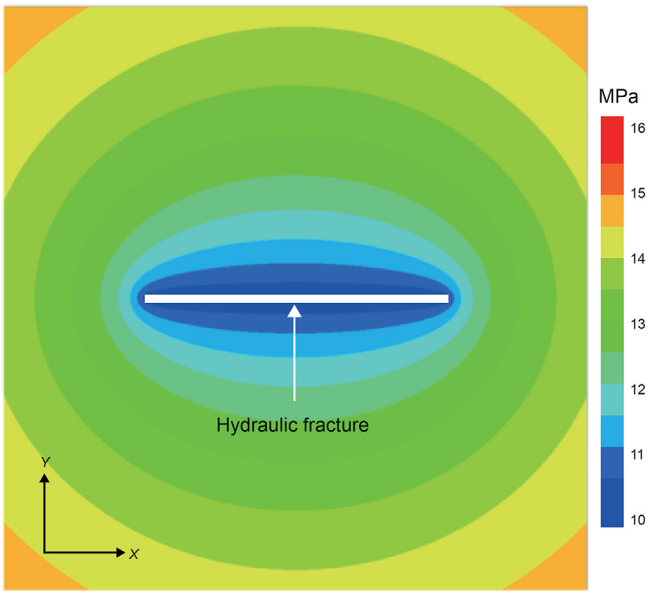

Fig. 10. Contour of the pore pressure for a single fracture producing for $\tau = 100$.

Second, the expansion of this reversal region is time dependent. It can be seen from Fig. 12a that the extent of the stress reversal region slightly decreases at early production time. This phenomenon can be explained by the action of opposing effects on the stress distribution between poroelastic and mechanical stress reorientation in the stress reversal region. Mechanical effect reorients stresses by applying more force to the fractures and, on the contrary, production induced stress reorientation is due to unloading (Fig. 13). Therefore, the maximum principal stress is redirected when the production begins, which causes the stress reversal region to shrink (Fig. 12b). The maximum stress will be fully reoriented within a fairly short time of production. Whereafter, the stress reversal region grows back with time. For large production times, poroelastic stress reorientation reaches a saturation plateau, so that there is a maximum value for the extent of stress reversal region during production.

Except the case in Fig. 12a, it has been studied that for different values of the stress deviator, fracture dimensions and dimensionless shear modulus ratio, the stress reversal region will have different sizes. The dimensionless time τ and ratio λ are used to illustrate the change of the stress reversal region extent over time. Fig. 14 demonstrate the evolution of the stress reversal region versus dimensionless time for different values of stress deviator. It is apparent from the results that the smaller deviator is, the larger the stress reversal region will be. However, the weight of all factors in the stress deviator can be different. The sensitivity of the extent of stress reversal to other parameters is thus smaller compared to the stress contrast. Therefore, for a stress reorientation to occur, a small initial horizontal stress contrast is necessary. The smaller the initial stress contrast is, the easier for the production induced stress will be to overcome the difference between the initial minimum and the maximum horizontal principal stresses.

As discussed previously, the stress deviator strongly affects the extent of the stress reversal region. Nevertheless, the factors included in the stress deviator have different impact on the curves of the dimensionless time versus extent of the stress reversal region. Fig. 15 shows that the magnitude of the depletion induced horizontal stress contrast firstly increases and subsequently stabilizes and remains constant. As the initial horizontal stress contrast increases, the decrease of the curves can be slower or for large production times the curves can be almost flat.

Pressure drawdown not only influences the extent of the stress reversal region, but also has effect on the timing of the occurrence of the maximum extent of the stress reversal region. One dimensional flow is known to be a good approximation for the flow in the middle of the fracture. In this case, solution for the diffusion equation that governs the pressure disturbance is,

$$P = \Delta P \cdot \mathrm{erfc}\left(\frac{x}{\sqrt{4ct}}\right) + P_0 \tag{16}$$

From the above equation, it is clear that different values of bottom hole pressure (or ΔP) can lead to different time instants, at which certain pressure disturbance magnitude reaches a point x. In addition, different mobility values also affect the saturation time of the isotropic point. This explains why the extent of the reorientation region will expand quicker when the mobility is higher (Fig. 16).

One of the aims of infill well optimization is that the stress reversal region can protect the parent well from the interference caused by the infill well. Thus, as the stress reversal region becomes larger, it is more likely that the protection can be achieved.

3.3. The case of multiple fractures

The impact of fracture spacing to stress reorientation is also investigated for a multi-fracture scenario. To simplify the problem, the fractures are considered to be parallel to each other. Fig. 17 show a single production well with two hydraulic fractures. Fig. 17a demonstrates that the two fractures are spaced at a distance that is equal to one half of the fracture length while the spacing in Fig. 17b equals to one eighth of the fracture length. Based on the maximum horizontal principal stress trajectories shown in Fig. 17a, one can observe that the stress reversal region of these two fractures is separated. The gap between the two stress reversal regions makes it possible that the infill well fractures can propagate and intersect the producer well. Due to effect of stress shadow, the stress reversal region of each fractures reduces compared to the single fracture case.

As shown in Fig. 17b, because the spacing between the two fractures is reduced, a continuous stress reversal region forms, which can deviate away the approaching infill well fractures. Therefore, an appropriate spacing of the fractures can help producer to form a stress shield against the secondary fractures from those infill wells.

4. Numerical results of infill well fracturing

The distinct element method is used to simulate the fracture propagation process under the effect of stress redistribution in the infill well fracturing treatment. As discussed previously, the fracture propagation is not only affected by the variations of stress field, but it is also influenced by the fracturing fluid and the injection schedule. Since the main goal of this study is to explore the impact of stress reorientation on fracture propagation, the properties of the reservoir are assumed to be constant except that the stress field after production is different in each simulation. The perturbed stress field is calculated in the reservoir model and imported into the hydraulic fracturing model.

Fig. 18 illustrates different time instants of infill well facture propagation with the well spacing of 170 m (Fig. 4), which includes the effect of stress reorientation. All the results show that when the fracture penetrates into the production zone, the width of the opening crack increases immediately and finally forms an asymmetric fracture which propagates away from the infill well along

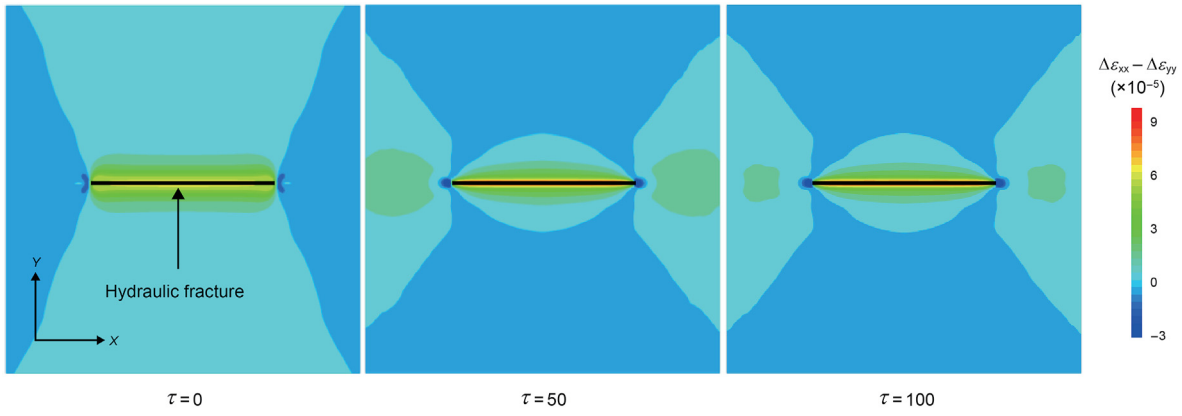

Fig. 11. Contour of the difference of strain incremental ($\Delta\varepsilon_{xx}-\Delta\varepsilon_{yy}$) around a single fracture, after $\tau = 0$, 50 and 100 of production.

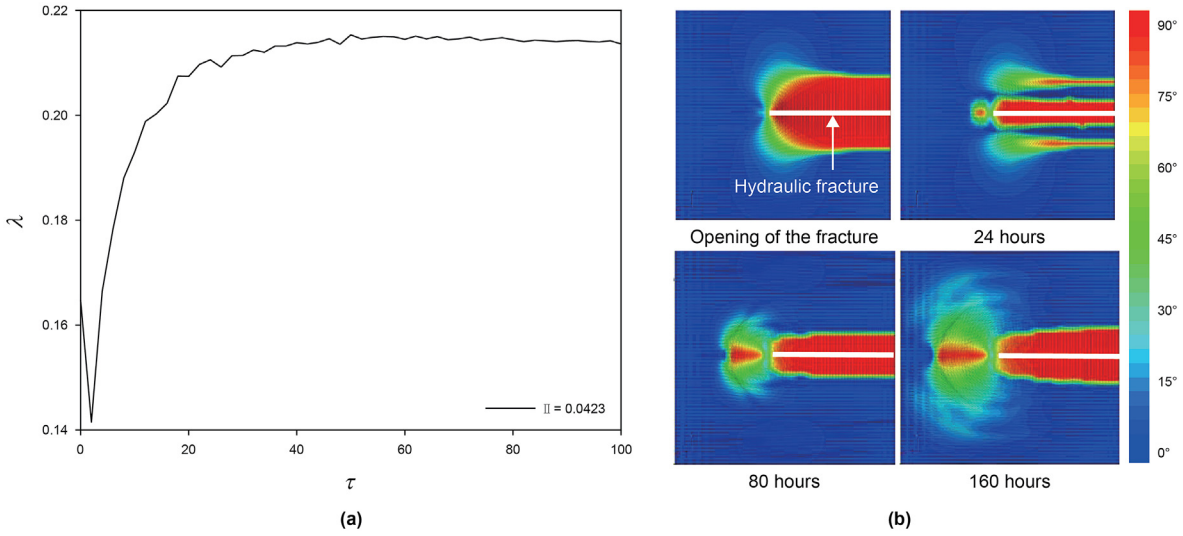

Fig. 12. a The extent of the stress reversal region for λ versus τ with $\Pi = 0.0423$, $\beta = 1$ and $\gamma = 0.2$, **b** reversal region's evolution from hydraulic fracture's opening to 160 h' production.

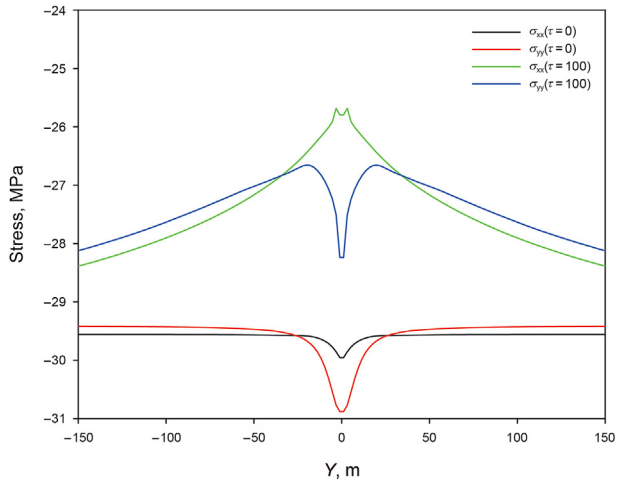

Fig. 13. Stress distribution curve for $\tau = 0$ and $\tau = 100$.

the x-axis. This is because the production causes an elliptical region with lower σ_{yy}, similar to the situation of fracture height growth into a low stress zone (Zhang and Dontsov, 2018). The small value of the closure stress makes the wing of the hydraulic fracture located in the depleted zone to be longer than the one located in the undepleted zone.

5. Discussion

One way to avoid the appearance of asymmetric fracture propagation is to adjust the inter-well spacing. Spacing the wells further away decreases pressure gradients and subsequently the risk of occurrence of asymmetric fractures in the infill well. As Fig. 19 demonstrates, after the infill well is placed 310 m away from the parent well rather than 170 m, the infill well fracture propagates more symmetrically compared to the last case. Nevertheless, some pitfalls can be identified quickly. First, altered stress field's range is significantly impacted by time, as illustrated in Fig. 14. So, the infill well drilling timing is connected to the parent well shutting time. Also, infill drilling is mainly considered in cases where well placement was initially dictated by leasing constraints. As it turns out, well spacing is not an easy parameter to adjust. But then other geomechanical considerations related to inter-well stress interference during stimulation would predominate as a result of the reduced well spacing (Roussel, 2011; Roussel and Sharma, 2010, 2012; Siebrits et al., 1998).

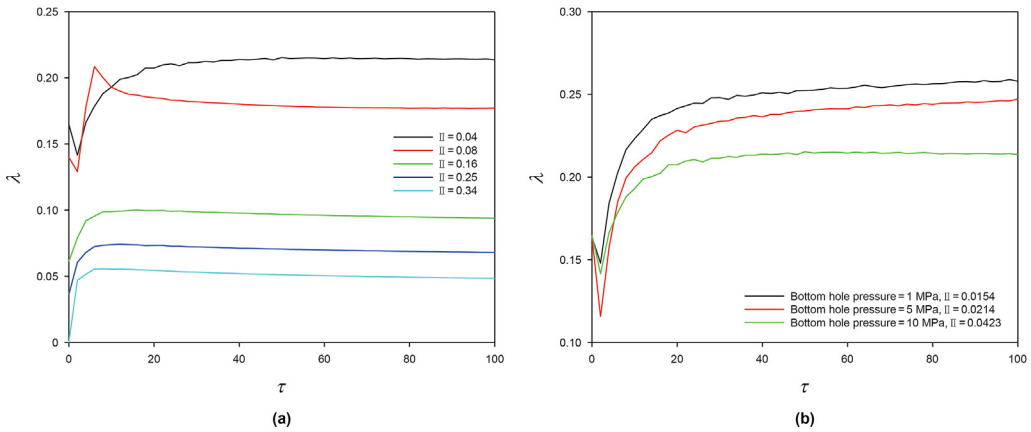

Fig. 14. **a** The extent of the stress reversal region for λ versus τ with different Π, $\beta = 1$ and $\gamma = 0.2$. **b** The extent of the stress reversal region for λ versus τ with different bottom hole pressure and different Π, $\beta = 1$ and $\gamma = 0.2$.

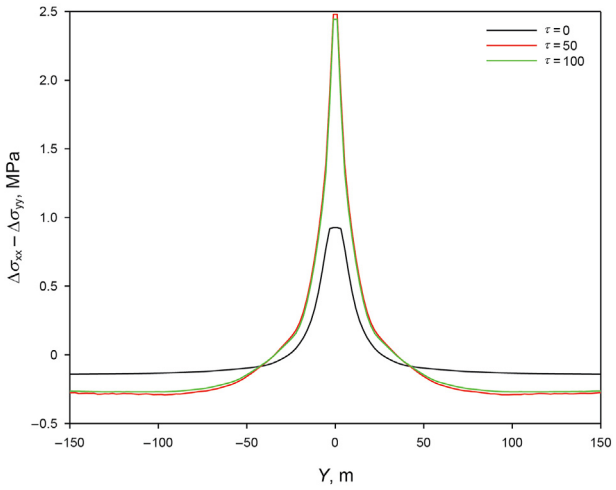

Fig. 15. The stress contrast along *y*-axis at different times.

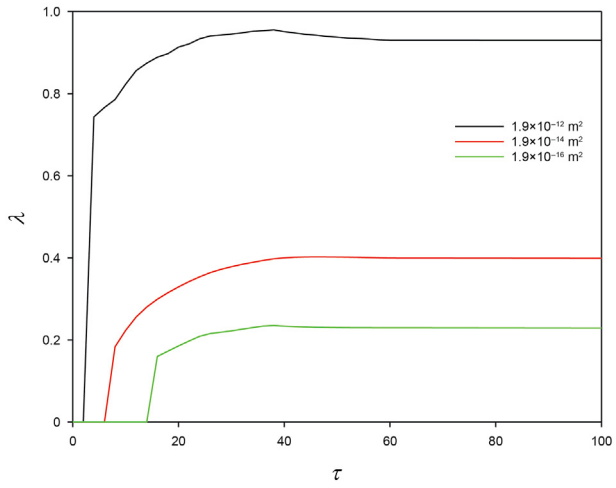

Fig. 16. The extent of the stress reversal region for λ versus τ for different values of permeability.

Another way to decrease pressure gradients responsible for stress decrease or reversal in the infill region would be by shutting-in the producing offset wells for some period of time before infilling (Gupta et al., 2012) or pre-loading the parent well as a defensive approach (Whitfield et al., 2018). While we have already verified the high sensitivity of stress induced by pore pressure decrease to the pressure drawdown, it is still unclear how long of a shut-in or pre-loading period would be required to reverse the direction and magnitude of the principal horizontal stresses back to their *in-situ* state and make the extent of the stress reversal region shrink. But considering the low permeability of shale reservoirs, it becomes uncertain that if the potential benefit from the stress redistribution would certainly prevail against the value lost from delaying production in the offset wells. Future work will be conducted to address these questions.

The onset time of stress reversal has large implications on the optimization of the moment when infill operations should be carried on. We already saw that past this time, asymmetric propagation of fractures initiated from the infill well, and consequently the volume of reservoir contacted by the stimulation, will be negatively affected. Production impacts not only the direction of principal horizontal stresses, but also the value of the horizontal stress contrast.

Previous studies showed that interactions between hydraulic and natural fractures are largely influenced by the stress regime in which the induced fracture propagates (Tang and Wu, 2018; Zhang et al., 2017). If the difference between minimum and maximum horizontal stresses is small, an induced fracture will have a larger tendency to branch-out when intersecting natural fractures, thus forming more complex fracture networks. There is a window of opportunity for improved stimulation efficiency if fracturing the infill well around (ideally slightly before) the time when principal horizontal stresses switch directions. As a result, infill operations should not be considered as an after-thought but instead an integral part of the field development plan right from the start, taking into consideration both the risk of fracturing an infill well past the onset time of stress reversal, and the opportunity for improved fracture complexity if stimulation takes place before that critical time.

6. Conclusions

This paper provides a case study to explore the time dependency of stress reorientation, as well as its behavior on problem parameters, such as threshold value of the horizontal stress

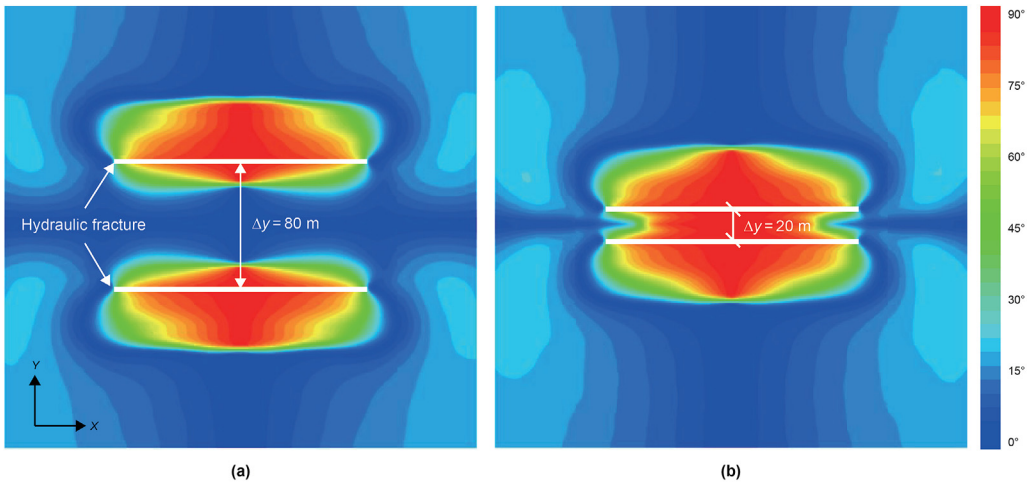

Fig. 17. Contour of the stress reorientation angle after production ($\tau = 100$) around two propped-open fractures **a** with fracture spacing equal to half of the fracture length, and **b** with fracture spacing equal to one eighth of fracture length.

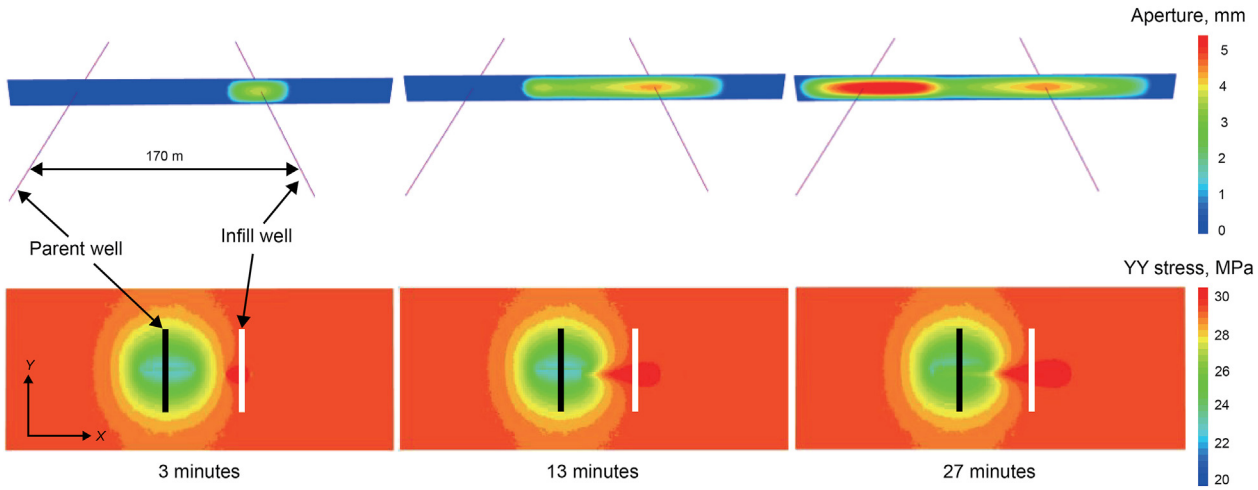

Fig. 18. Top: contour of the infill well fracture aperture at different time instants of injection; bottom: contour of YY-stress at different time instants of injection.

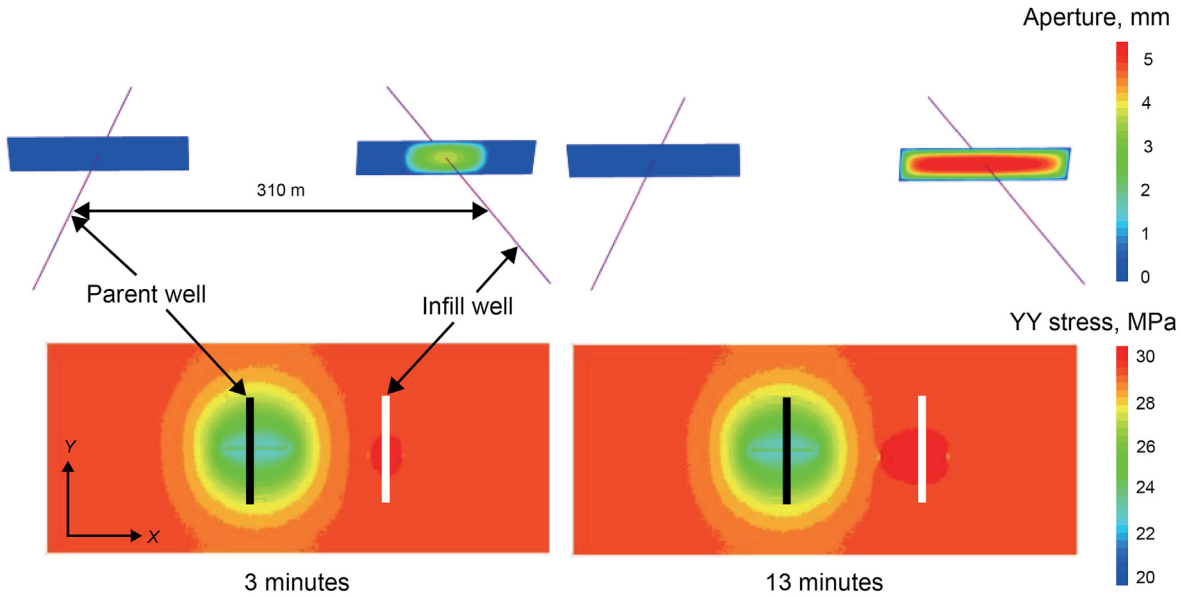

Fig. 19. Top: contour of the infill well fracture aperture at different time instants of injection, bottom: contour of YY-stress at different time instants of injection. The infill well spacing is increased to 310 m, compared with the model in Fig. 18.

contrast, the influence of stress deviator, dimensionless shear ratio, dimensionless fracture size and mechanical properties of the reservoir. The reservoir simulation is computed using the finite difference method, which considers both poroelastic effect and mechanical effect on the stress redistribution. The increase of pressure drawdown by decreasing bottom hole pressure and increasing mobility can expand the stress reversal region. The value of the initial horizontal stress contrast is the primary factor for stress reorientation.

Fracture propagation during stimulation of the infill well is studied using the distinct element method. Results show that the decrease of the horizontal stresses around the parent well lead to asymmetrical propagation of a hydraulic fracture of the infill well. The width of the fracture in the vicinity of the parent well is also much larger compared to the width near the infill well. The asymmetrical propagation of the infill well hydraulic fracture confirms that it is necessary to consider the temporal and spatial effects when optimizing the completion of the infill well treatments.

Acknowledgment

The authors acknowledge the support provided by the Scientific Research and Technology Development Project of CNPC (Grant No. kt2017-19-01-1), the National Natural Science Foundation of China (Grant No. 41772286, No. 42077247 and No. 42002271), and PetroChina Innovation Foundation (Grant No. 2018D-5007-0202), and Project funded by China Postdoctoral Science Foundation (Grant No. 2021T140514), and Open Research Fund of State Key Laboratory of Geomechanics and Geotechnical Engineering, Institute of Rock and Soil Mechanics, Chinese Academy of Sciences (Grant No. Z020009). The useful discussion with Branko Damjanac from Itasca Consulting Group is also greatly appreciated.

References

Aghighi, M.A., Rahman, S.S., Rahman, M.M., 2009. Effect of formation stress distribution on hydraulic fracture reorientation in tight gas sands. In: SPE Asia Pacific Oil and Gas Conference and Exhibition, 4–6 August, Jakarta, Indonesia. https://doi.org/10.2118/122723-MS.

Ajani, A., Kelkar, M., 2012. Interference study in shale plays. In: SPE Hydraulic Fracturing Technology Conference, 6–8 February, the Woodlands, Texas. https://doi.org/10.2118/151045-ms.

Berchenko, I., Detournay, E., 1997. Deviation of hydraulic fractures through poroelastic stress changes induced by fluid injection and pumping. Int. J. Rock Mech. Min. Sci. 34 (6), 1009–1019. https://doi.org/10.1016/S1365-1609(97)80010-X.

Biot, M.A., 1955. Theory of elasticity and consolidation for a porous anisotropic solid. J. Appl. Phys. 26 (2), 182–185. https://doi.org/10.1063/1.1721956.

Bruno, M.S., Nakagawa, F.M., 1991. Pore pressure influence on tensile fracture propagation in sedimentary rock. Int. J. Rock Mech. Min. Sci. Geomech. Abstr. 28 (4), 261–273. https://doi.org/10.1016/0148-9062(91)90593-B.

Chen, H.Y., Teufel, L.W., 2001. Reservoir stress changes induced by production/injection. In: SPE Rocky Mountain Petroleum Technology Conference. 21–23 May, Keystone, Colorado. https://doi.org/10.2118/71087-MS.

Cundall, P.A., 1988. Formulation of a three-dimensional distinct element model—Part I. A scheme to detect and represent contacts in a system composed of many polyhedral blocks. Int. J. Rock Mech. Min. Sci. Geomech. Abstr. 25 (3), 107–116. https://doi.org/10.1016/0148-9062(88)92293-0.

Elbel, J.L., Mack, M.G., 1993. Refracturing: observations and theories. In: SPE Production Operations Symposium, 21–23 March, Oklahoma City, Oklahoma. https://doi.org/10.2118/25464-MS.

Gao, Q., Cheng, Y.F., Han, S.C., et al., 2019. Numerical modeling of hydraulic fracture propagation behaviors influenced by pre-existing injection and production wells. J. Petrol. Sci. Eng. 172, 976–987. https://doi.org/10.1016/j.petrol.2018.09.005.

Gupta, J.K., Zielonka, M.G., Albert, R.A., et al., 2012. Integrated methodology for optimizing development of unconventional gas resources. In: SPE Hydraulic Fracturing Technology Conference, 6–8 February, the Woodlands, Texas. https://doi.org/10.2118/152224-MS.

Hart, R., Cundall, P.A., Lemos, J., 1988. Formulation of a three-dimensional distinct element model—Part II. Mechanical calculations for motion and interaction of a system composed of many polyhedral blocks. Int. J. Rock Mech. Min. Sci. Geomech. Abstr. 25 (3), 117–125. https://doi.org/10.1016/0148-9062(88)92294-2.

Huang, L.K., Liu, J.J., Zhang, F.S., et al., 2019. Exploring the influence of rock inherent heterogeneity and grain size on hydraulic fracturing using discrete element modeling. Int. J. Solid Struct. 176, 207–220. https://doi.org/10.1016/j.ijsolstr.2019.06.018.

Huang, L.K., Liu, J.J., Zhang, F.S., et al., 2020. 3D lattice modeling of hydraulic fracture initiation and near-wellbore propagation for different perforation models. J. Petrol. Sci. Eng. 191. https://doi.org/10.1016/j.petrol.2020.107169.

Itasca Consulting Group Inc, 2011. FLAC3D (Fast Lagrangian Analysis of Continua in 3 Dimensions) Version 5.0. Minneapolis, Minnesota, United States.

Itasca Consulting Group Inc, 2016. 3DEC (Three-Dimensional Numerical Modeling Code) Version 5.2. Minneapolis, Minnesota, United States.

Li, P.C., Song, Z.Y., Wu, Z.Z., 2006. Study on reorientation mechanism of refracturing in Ordos Basin - a case study: chang 6 formation, Yanchang group, Triassic system in Wangyao section of Ansai oil field. In: International Oil and Gas Conference and Exhibition in China, 5–7 December, Beijing, China. https://doi.org/10.2118/104260-ms.

Li, X., Wang, J.H., Elsworth, D., 2017. Stress redistribution and fracture propagation during restimulation of gas shale reservoirs. J. Petrol. Sci. Eng. 154, 150–160. https://doi.org/10.1016/j.petrol.2017.04.027.

Lin, B.T., Meng, H., Pan, J.J., et al., 2020. Porothermoelastic response of an oil sand formation subjected to injection and micro-fracturing in horizontal wells. Petrol. Sci. 17, 687–700. https://doi.org/10.1007/s12182-019-00420-1.

Mack, M.G., Elbel, J.L., 1994. Hydraulic fracture orientation and pressure response during fracturing of producing wells. In: 1st North American Rock Mechanics Symposium, 1–3 June, Austin, Texas.

Roussel, N.P., 2011. Stress Reorientation in Low Permeability Reservoirs. The University of Texas at Austin.

Roussel, N.P., Sharma, M.M., 2010. Quantifying transient effects in altered-stress refracturing of vertical wells. SPE J. 15 (3), 770–782. https://doi.org/10.2118/119522-PA.

Roussel, N.P., Sharma, M.M., 2012. Role of stress reorientation in the success of refracture treatments in tight gas sands. SPE Prod. Oper. 27 (4), 346–355. https://doi.org/10.2118/134491-PA.

Safari, R., Lewis, R., Ma, X.D., et al., 2017. Infill-well fracturing optimization in tightly spaced horizontal wells. SPE J. 22 (2), 582–595. https://doi.org/10.2118/178513-PA.

Sahai, V., Jackson, G., Rai, R., et al., 2012. Optimal well spacing configurations for unconventional gas reservoirs. In: SPE Americas Unconventional Resources Conference, 5–7 June, Pittsburgh, Pennsylvania USA. https://doi.org/10.2118/155751-MS.

Siebrits, E., Elbel, J.L., Detournay, E., et al., 1998. Parameters affecting azimuth and length of a secondary fracture during a refracture treatment. In: SPE Annual Technical Conference and Exhibition, 27–30 September, New Orleans, Louisiana. https://doi.org/10.2118/48928-MS.

Tan, P., Jin, Y., Pang, H.W., 2021. Hydraulic fracture vertical propagation behavior in transversely isotropic layered shale formation with transition zone using XFEM-based CZM method. Eng. Fract. Mech. 248. https://doi.org/10.1016/j.engfracmech.2021.107707.

Tan, P., Pang, H.W., Zhang, R.X., et al., 2020. Experimental investigation into hydraulic fracture geometry and proppant migration characteristics for southeastern Sichuan deep shale reservoirs. J. Petrol. Sci. Eng. 184. https://doi.org/10.1016/j.petrol.2019.106517.

Tang, J.Z., Wu, K., 2018. A 3-D model for simulation of weak interface slippage for fracture height containment in shale reservoirs. Int. J. Solid Struct. 144, 248–264. https://doi.org/10.1016/j.ijsolstr.2018.05.007.

Tang, X.H., Rutqvist, J., Hu, M.S., et al., 2019. Modeling three-dimensional fluid-driven propagation of multiple fractures using TOUGH-FEMM. Rock Mech. Rock Eng. 52 (2), 611–627. https://doi.org/10.1007/s00603-018-1715-7.

Warpinski, N.R., Branagan, P.T., 1989. Altered-stress fracturing. J. Petrol. Technol. 41 (9), 990–997. https://doi.org/10.2118/17533-PA.

Whitfield, T., Watkins, M.H., Dickinson, L.J., 2018. Pre-loads: successful mitigation of damaging frac hits in the eagle ford. In: SPE Annual Technical Conference and Exhibition, 24–26 September, Dallas, Texas. https://doi.org/10.2118/191712-ms.

Yi, L.P., Waisman, H., Yang, Z.Z., et al., 2020. A consistent phase field model for hydraulic fracture propagation in poroelastic media. Comput. Methods Appl. Mech. Eng. 372. https://doi.org/10.1016/j.cma.2020.113396.

Yin, Z.R., Huang, H.W., Zhang, F.S., et al., 2020. Three dimensional distinct element modeling of fault reactivation and induced seismicity due to hydraulic fracturing injection and flowback. J. Rock Mech. Geotech. Eng. 12 (4), 752–767. https://doi.org/10.1016/j.jrmge.2019.12.009.

Zeng, Y.J., Zhang, X., Zhang, B.P., 2015. Stress redistribution in multi-stage hydraulic fracturing of horizontal wells in shales. Petrol. Sci. 12 (4), 628–635. https://doi.org/10.1007/s12182-015-0048-3.

Zhai, Z.Y., Sharma, M.M., 2007. Estimating fracture reorientation due to long term fluid injection/production. In: Production and Operations Symposium, 31 March–3 April, Oklahoma City, Oklahoma. https://doi.org/10.2118/106387-MS.

Zhang, F.S., Damjanac, B., Maxwell, S., 2019. Investigating hydraulic fracturing complexity in naturally fractured rock masses using fully coupled multiscale numerical modeling. Rock Mech. Rock Eng. 52, 5137–5160. https://doi.org/10.1007/s00603-019-01851-3.

Zhang, F.S., Dontsov, E., 2018. Modeling hydraulic fracture propagation and proppant transport in a two-layer formation with stress drop. Eng. Fract. Mech. 199, 705–720. https://doi.org/10.1016/j.engfracmech.2018.07.008.

Zhang, F.S., Dontsov, E., Mack, M., 2017. Fully coupled simulation of a hydraulic fracture interacting with natural fractures with a hybrid discrete-continuum method. Int. J. Numer. Anal. Methods GeoMech. 41, 1430–1452. https://

doi.org/10.1002/nag.2682.
Zhang, F.S., Mack, M., 2017. Integrating fully coupled geomechanical modeling with microsesmicity for the analysis of refracturing treatment. J. Nat. Gas Sci. Eng. 46, 16–25. https://doi.org/10.1016/j.jngse.2017.07.008.
Zhang, S.C., Lei, X., Zhou, Y.S., et al., 2015. Numerical simulation of hydraulic fracture propagation in tight oil reservoirs by volumetric fracturing. Petrol. Sci. 12 (4), 674–682. https://doi.org/10.1007/s12182-015-0055-4.
Zhu, H.Y., Tang, X.H., Song, Y.J., et al., 2021. An infill well fracturing model and its microseismic events barrier effect: a case in fuling shale gas reservoir. SPE J. 26 (1), 113–134. https://doi.org/10.2118/202485-PA.